Contact Fatigue Crack Initiation Prediction of Spur Gears Based on Finite Element Dynamics Analysis

W. J. Qin[1] and C. Y. Guan[2]

[1] School of Mechanical Engineering, Beijing Institute of Technology, Beijing, China, 100081 E-mail: qinwj@bit.edu.cn

ABSTRACT. *The methods of contact stress analysis and fatigue crack initiation prediction of gears are presented and applied to a pair of spur gears in a high speed diesel engine in this paper. The surface and subsurface stresses of the gear tooth is investigated using Hertzian theory and finite element method. The effects of friction and speed are analysed. It is found that friction will increases the von Mises stresses and change the shear stress cycles so that the surface pitting is more likely to form with the increase of friction. It is also found that the stresses of the points near the engagement and recess areas are very great, and with the improvement of speed the stresses fluctuate more severely and these zones become more dangerous and resulted lower fatigue lives compared with static contact conditions.*

1 INTRODUCTION

Under normal operating conditions, contact fatigue (often associated with surface pitting) is one of the most common failure modes for gear tooth surfaces[1-3], which is commonly attributed to the repeated rolling and sliding contact loads. In gears with fine surface finish and good lubrication, the contact compression and shear stresses play a dominant role in a fatigue crack initiation process. These contact stresses are generally the highest at some distance under the surface, where the initial crack appearance is most likely[4-6].

Usually, the stress field of each material point is simulated analytically by applying moving Hertzian contact pressure and Coulomb friction[7-9]. Recently, the finite element method is more and more used to simulated the real rolling and sliding contact and more precise stress results are expected to be obtained[10-15]. As the impact of engagement is considered, the finite element dynamic contact analysis is necessary to investigate the stresses at various speeds.

When the stress loading cycles are determined, the number of stress cycles required for a fatigue crack to appear can be determined. Rolling contact fatigue is typically a multiaxial fatigue mechanism and several methods have been developed such as Smith-Watson-Topper (SWT) method, Coffin–Manson's hypothesis (ε-N method) and Basquin equation based on equivalent stress (σ-N method) [16-18].

In this paper, the methods of contact stress analysis and fatigue crack initiation prediction of gears are presented and applied to a pair of spur gears in a high speed

diesel engine. The stresses and numbers of loading cycles required for fatigue crack initiation at different positions and different speeds are investigated.

2 CALCULATION OF CONTACT STRESSES

2.1 *Hertzian Method*

Contact stresses of gears are often calculated with use of Hertzian theory by applying the equivalent contact cylinders generated from the curvature radii at the contact point. The two-dimensional distribution of normal contact pressure in the contact area is determined as[5]

$$p(x)=\frac{2P}{\pi a}\sqrt{1-\frac{x^2}{a^2}} \tag{1}$$

where P is the compression load per unit axial length and a is the semi-contact-width.

According to an elastic half-space loaded over the strip ($e<x<f$) by a normal pressure $p(s)$ distributed, the stress components at point $A(x, z)$ are:

$$\begin{cases}\sigma_x=\dfrac{-2z}{\pi}\displaystyle\int_{-e}^{f}\frac{p(s)(x-s)^2ds}{[(x-s)^2+z^2]^2}\\ \sigma_z=\dfrac{-2z^3}{\pi}\displaystyle\int_{-e}^{f}\frac{p(s)ds}{[(x-s)^2+z^2]^2}\\ \tau_{xy}=\dfrac{-2z^2}{\pi}\displaystyle\int_{-e}^{f}\frac{p(s)(x-s)ds}{[(x-s)^2+z^2]^2}\end{cases} \tag{2}$$

Applying the normal contact pressure in Eq. (1) to Eq. (2), the two-dimensional stresses of any point in the contact bodies can be obtained. Taking $\upsilon=0.3$, the von Mises equivalent stress gets to its maximum value $0.558p_0$ at the position of $0.7a$ below the contact point and τ_{xz} gets to its maximum value $0.25p_0$ at the points ($\pm0.87a$,$0.50a$), where p_0 is the maximum contact pressure.

2.2 *Finite Element Dynamics Analysis*

As mesh impact caused by the backlash and the approach and recess of tooth meshing is concerned, explicit method is suitable to solve this impact-contact problem[19-21], and a penalty method is used in contact constraints.

2.2.1 *Explicit method*

A central difference rule is widely used in explicit method to integrate the equations of motion (3) explicitly through time, using the kinematic conditions at one increment to calculate the kinematic conditions at the next increment[22].

$$\boldsymbol{M}\ddot{\boldsymbol{u}}=\boldsymbol{F}-\boldsymbol{I} \tag{3}$$

where $\boldsymbol{M}$ is the diagonal lumped mass matrix, $\boldsymbol{F}$ is the applied load vector, and $\boldsymbol{I}$ is the internal force vector.

The accelerations at the beginning of the current increment (time t) are calculated as

$$\ddot{\boldsymbol{u}}\big|_{(t)}=\boldsymbol{M}^{-1}(\boldsymbol{F}-\boldsymbol{I})\big|_{(t)} \tag{4}$$

The velocities at the middle of the current increment is determined by:

$$\dot{\boldsymbol{u}}\big|_{(t+\frac{\Delta t}{2})} = \dot{\boldsymbol{u}}\big|_{(t-\frac{\Delta t}{2})} + \frac{(\triangle t\big|_{(t+\Delta t)} + \triangle t\big|_{(t)})}{2}\ddot{\boldsymbol{u}}\big|_{(t)} \tag{5}$$

The velocities are integrated through time and added to the displacements at the beginning of the increment to determine the displacements at the end of the increment:

$$\boldsymbol{u}\big|_{(t+\Delta t)} = \boldsymbol{u}\big|_{(t)} + \triangle t\big|_{(t+\Delta t)}\dot{\boldsymbol{u}}\big|_{(t+\frac{\Delta t}{2})} \tag{6}$$

2.2.2 *Penalty contact method*

A penalty contact method searches for node-into-face and edge-into-edge penetrations in the current configuration. For node-to-face contact, forces that are a function of the penetration distance are applied to the slave nodes to oppose the penetration, while equal and opposite forces act on the master surface at the penetration point. The master surface contact forces are distributed to the nodes of the master faces being penetrated. For edge-to-edge contact, the opposing contact forces are distributed to the nodes of the two contacting edges. The value of the contact force is proportional to the penetration and the penalty factor which represents the contact stiffness. This method corresponds to enforcement a spring between the slave nodes and master nodes against their penetration[22,23].

3 PREDICTION OF CONTACT FATIGUE CRACK INITIATION

Smith and co-authors proposed a simple form of a damage parameter, SWT, described as stress and strain product $\sigma_{max}\varepsilon_a$ for fatigue life determination under uniaxial tension-compression. The most popular form of SWT parameter in the critical plane is that proposed by Socie in the plane of maximum normal strain range $\Delta\varepsilon_1$[20]

$$\sigma_{\max}\frac{\Delta\varepsilon_1}{2} = \frac{\sigma_f'^{\,2}}{2}(2N_f)^{2b} + \sigma_f'\varepsilon_f'(2N_f)^{b+c} \tag{7}$$

where is the maximum normal stress on the critical plane.

4 ANALYSIS OF CONTACT STRESS FOR THE SPUR GEAR PAIR

In this paper, Abaqus/Explicit is applied to simulate the process from engagement to recess of a pair of spur gear teeth in one diesel engine at the low speed (600r/min) and high speed (1200r/min) respectively. The basic data of the spur gear geometry is listed in Table1, and the material parameters is listed in Table2.

Table 1 the basic data of the spur gear geometry

	Number of teeth	Module (mm)	Pressure angle(°)	Coefficient of profile	Tooth width(mm)
Driving gear	47	2.5	20	0.10159	20
Driven gear	47	2.5	20	0.10159	20

Table 2 The material parameters of the gear

Material	Tensile strength σ_T (MPa)	Yield limit σ_s (MPa)	Fatigue strength coefficient σ_f' (MPa)	Fatigue ductility coefficient ε_f'	Strength exponent b	Fatigue ductility exponent c
42CrMo4V	1134	880	1820	0.65	-0.08	-0.76

4.1 ***FEM Model of the Gear Pair***

The gear pair is meshed using hexahedron element as shown in Fig.1. The half contact width is about 0.20mm, so the local element size of the contact area is defined as 0.05mm as shown in Fig. 2. The radial and axial displacements of the surface of the shaft hole of each gear are fixed. The rotation speed is applied on the surface of the shaft hole of the driving gear and the torque is applied on that of the driven gear. Contact constraints are applied on the surfaces of the meshing teeth.

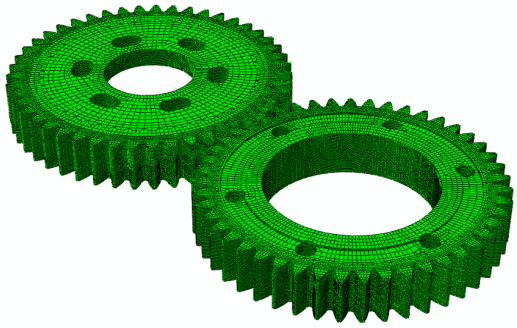

Fig.1 Meshed gear pair

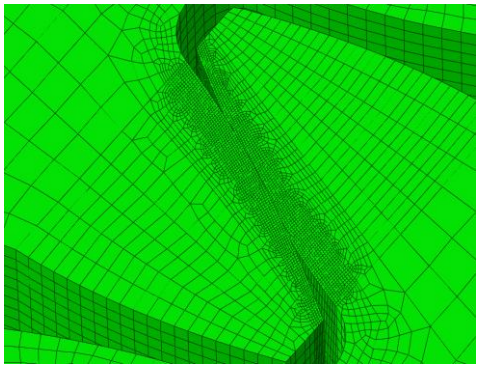

Fig. 2 Local mesh of contact tooth pair

4.2 ***Stress Results on and Under the Surface***

The von Mises equivalent stress distribution of one contact tooth pair meshing near the pitch circle at the low speed (600r/min) and under no friction condition is shown in Fig.3. Fig. 4 gives the cycles of shear stress within the middle-width plane of points at various depths under the surface of the contact point. The maximum stresses and their depths compared with those calculated by Hertzian theory using static load are listed in Table 3. It can be seen that the maximum stress values calculated from FEM are close to the statics Hertizen values at the low speed.

Table 3 Maximum stresses compared with those calculated by Hertzian theory

	Von Mises stress		Shear Stress	
	Value (MPa)	Depth (mm)	Value (MPa)	Depth (mm)
FEM value	690.5	0.125	265.6	0.100
Hertzian value	600.4	0.130	271.5	0.093

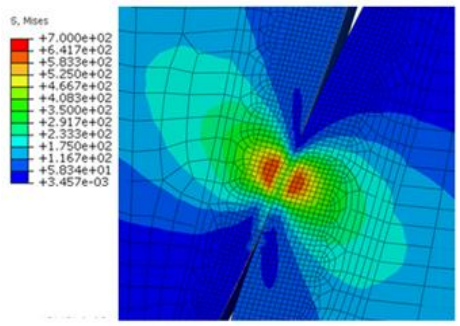

Fig.3 Von Mises stress distribution (μ = 0. 0)

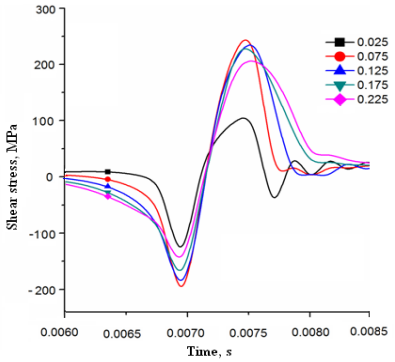

Fig. 4 Shear stress cycles (μ = 0. 0)

4.3 ***Effects of Friction on Stresses***

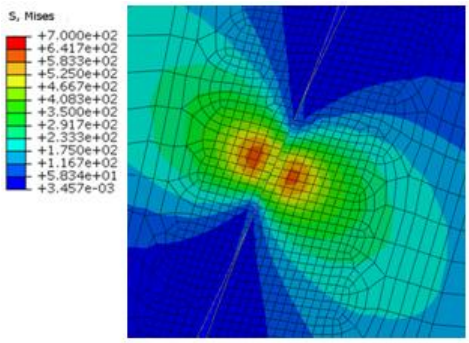

(a) μ =0.1

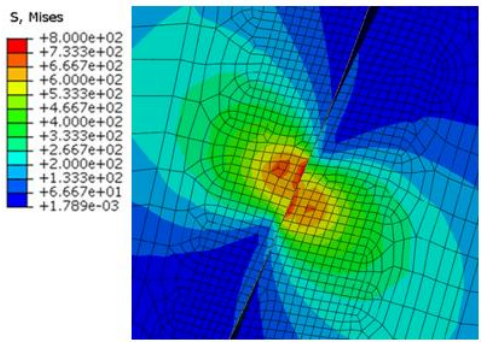

(b) μ=0.3

Fig. 5 Von Mises stress distributions with different friction

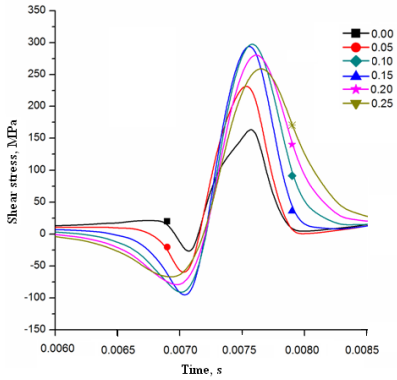

(a) μ =0.1

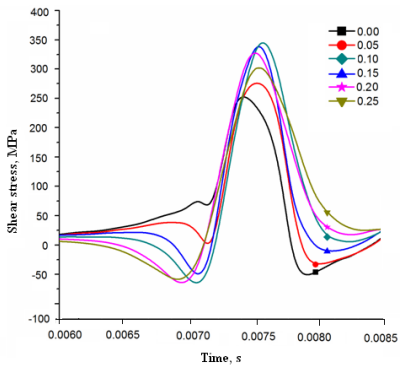

(b) μ=0.3

Fig. 6 Shear stress cycles on and under the contact surface with different friction

Friction will cause the tangential pressure on the surface and influence the values and distributions of contact stresses. Fig. 5 is the von Mises stress distributions on the contact surface point of the same location in Fig. 3 when the friction coefficient μ = 0.1 and μ = 0.3 respectively. It can be seen that the von Mises stress distributions change

significantly with the increase of frictions, and the greatest stress point is on the surface because of the greater shear stress. Fig. 6(a) and Fig. 6(b) are the shear stress cycles on and under the contact surface at different depths when the friction coefficient μ = 0.1 and μ = 0.3. It can be seen that the positive shear stress values become greater while the negative values become smaller with the friction increases due to the imposition of positive shear stress caused by the tangential pressure, and this change is more obvious near the surface.

4.4 *Dynamic Contact Stresses at Different Speeds*

As for the gear pair studied in this paper, the profile of a gear tooth can be divided into double tooth contact area and single tooth contact area. Considering a tooth in the driving gear, the area near the root and top are the double tooth contact areas and that near the pitch circle is the single tooth contact area as shown in Fig. 7. In a statics analysis, the load on the single tooth contact area is higher than those of the double tooth contact area, so the area near the pitch circle is often thought to be most dangerous to damage. But in a dynamics analysis, the loads on the area near the engagement and recess zones may be very high, even greater than the load on the single tooth contact area due to the sudden loading impacts. Therefore, the areas near the root and top of the tooth are also dangerous to damage and must be included in consideration.

The maximum von Mises stress histories from engagement to recess (from point A to point C) at 600r/min and 1200r/min are shown in Fig. 8. It can be seen that the maximum von Mises stresses of the points near the engagement and recess areas are greater than those of points near the pitch circle. With the improvement of speed, the impacts become greater, so the curve fluctuates more severely and the stresses of points near the engagement and recess become even greater. The introduction of profile relief can reduce the contact pressure at these critical points[15].

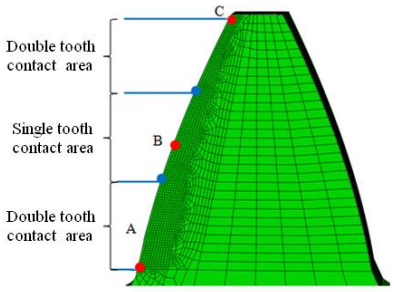

Fig. 7 Contact areas and characteristic points

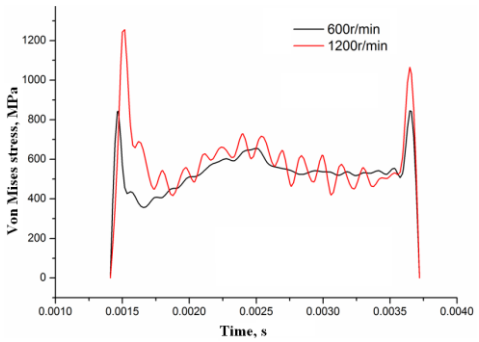

Fig. 8 Von Mises stress histories

5 CRACK INITIATION PREDICTION

5.1 *Number of Load Cycles for Crack Initiation with Various Friction Coefficients*

Using the results in Section 4.2 and Section 4.3, the number of load cycles for crack initiation of points on and under the contact surface at the low speed (600r/min) when

the friction coefficient μ=0.0, μ=0.1 and μ=0.3 are calculated and shown in Fig.9. It can be seen that the least fatigue life decreases while the corresponding position goes up to the surface with the increase of friction. So the surface pitting is more likely to form when friction is greater.

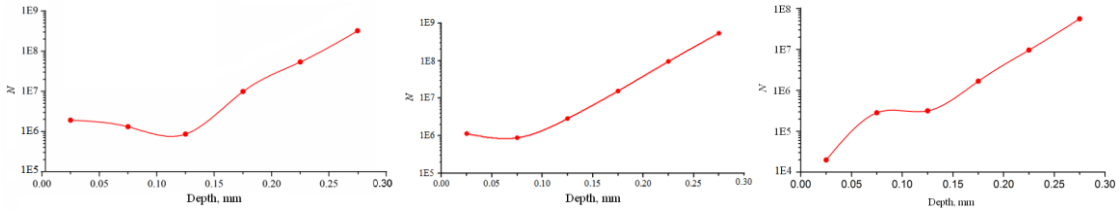

(a) μ=0.0 (b) μ=0.1 (c) μ=0.3

Fig.9 Fatigue lives with various friction coefficients

5.2 ***Number of Load Cycles for Crack Initiation at Different Speeds***

From the stress results in Section 4.4, it can be seen that the maximum von Mises stresses of Point A and Point C at the speed 1200r/min are greater than the yield limit of the material. Elasticity- plasticity FEM analysis is carried out and the strain components of Point A, Point B and Point C on the driving gear at speeds of 600r/min and 1200r/min are obtained and the calculated fatigue lives are listed in Table 4. It can be seen that impacts result in lower fatigue lives at the points near the engagement and recess area. With the improvement of speed, the points at these positions become more dangerous while the life of the point near the pitch circle shows a little change.

Table 4 Fatigue lives (number of load cycles)

Speed(r/min)	Point A	Point B	Point C
600	1.37E5	8.26E5	1.03E5
1200	1.68E4	8.18E5	2.35E4

6 CONCLUSIONS

As the stresses on and under the surface are concerned, the von Mises stresses and shear stresses increase along the depth firstly, and then decreased after getting to the maximum values. Friction influences the values and distributions of contact stresses by increases the von Mises stresses and change the shear stress cycles with the increase of friction. These changes are more obvious near the surface. The least fatigue life decreases while the corresponding position goes up to the surface with the increase of friction so that the surface pitting is more likely to form when friction is greater.

In a statics analysis, the load on the single tooth contact area is higher than those of the double tooth contact area because all the torque is applied on the single tooth pair. In a dynamics analysis, the loads on the area near the engagement and recess zones are

much greater than the static loads due to the sudden loading impacts. Therefore, the stresses of the points near the engagement and recess areas are also greater compared to those near the pitch circle. With the improvement of speed, the stresses fluctuate more severely and the points near the engagement and recess become more dangerous and result in lower fatigue lives compared with static contact conditions.

REFERENCES

1. Yan Ding, Neville F. Rieger. (2003) *Wear* 254, 1307-1317.
2. A. C. BATISTA, A. M. DIAS, J. L . LEBRUN, J. C. L E F LOUR and G. INGLEBERT. (2000) *Fatigue Fract Engng Mater Struct* 23, 217-228.
3. P. J. L. Fernands, C. McDuling. (1997) *Engineering Failure Analysis* 4(2), 99-107.
4. S. Glodez Ï, Z. Ren, J. Flas Ïker. (1999) *Computers and Structures* 73, 475-483.
5. Johnson, K. L. (1985) In: *Contact Mechanics*, Cambridge University Press, Cambridge
6. Editorial board of handbook of mechanical design. (2009) In: *Design of Fatigue Strength*, China Machine Press, Beiging.
7. K. Aslantas, S. Tasgetiren. (2004) *Wear* 257, 1167-1175.
8. J. Flašker, G. Fajdiga, S. Glodež, T. K. Hellen (2001) *Int J Fatigue* 23, 599-605.
9. M. Šraml, J. Flašker. (2007) *Int J Adv Manuf Technol* 31, 1066-1075.
10. F. L. Litvin, A. Fuentes, I. Gonzalez-Perez, L. Carnevali, T.M. Sep. (2002) *Comput. Methods Appl. Mech. Engrg* 191, 5707-5740.
11. M. Šraml, J. Flašker, I. Potrc. (2003) *International Journal of Fatigue* 25, 585-595.
12. Y. T. Tian, C. X. Li, W. Tong, C. H. Wu. (2003) *Journal of Mechanical Design* 125, 625-631.
13. A. R. Hassan. (2009) *Engineering and Technology* 34, 611-616.
14. K. Mao. (2007) *Wear* 262, 1281-1288.
15. T. Osman, P. Velex. (2012) *Tribology International* 46, 84-96.
16. M. Ciavarella, F.Monno. (2010) *Tribology International* 43, 2139-2144.
17. D. G. Shang, D. J. Wang.(2007) In: *Multiaxial fatigue strength*, Science Press, Beijing.
18. S. Suresh.(1998) In: *Fatigue of Materials*, Second Edition, Cambridge University Press, Cambridge.
19. R. F. Li, J. J. Wang. (1997) In: *gear system dynamics*, Science Press, Beijing.
20. T. J. Lin, H. Ou, R. F. Li. (2007) *Comput. Methods Appl. Mech. Engrg.* 196, 1716-1728.
21. T. Belyscchko, W. K. Liu, B. Moran. (2000) In: *Nonlinear Finite Elements for Continua and Structures*, John Wiley & Sons Ltd.
22. Dassault Systèmes. *Abaqus Analysis User's Manual*, Version 6.8
23. Y. Zhong, Z. H. Zhong, G. Y. Li, G. Y. Sun, F. X. Xu. (2011) *Journal of Mechanical Engineering* 47(13) 44-58